JOURNAL OF MATERIALS SCIENCE **39** (2004) 6495–6502

The effect of cold work on the precipitation kinetics of AA6111 aluminum

G.K. QUAINOO*, S. YANNACOPOULOS‡
Department of Mechanical Engineering, University of Saskatchewan, 57 Campus Drive, Saskatoon, SK., S7N 5A9
E-mail: spiro@engr.usask.ca

In the automotive industry, the drive to meet Corporate Average Fuel Efficiency (CAFE) standards has resulted in the need to reduce vehicular weight in new automobile designs. One effective method has been to use lighter materials such as aluminum alloys in outer body panels. Heat treatable AA6111 is one of the materials being employed in outer body panels due to its unique combination of formability, paint bake strengthening and superior corrosion resistance characteristics. For a formed and painted automobile panel, the final mechanical properties involve a combination of strength components arising from cold work, strain aging, precipitation and recovery. The challenge is to find a method of quantifying each of these strength components.

In this study, the effect of cold work on the precipitation kinetics of AA6111 has been evaluated, by means of tensile testing, differential scanning calorimetry (DSC), and transmission electron microscopy (TEM). The results show a considerable improvement in yield and tensile strength with increasing level of cold work. DSC showed acceleration in the precipitation kinetics of the alloy with increasing level of cold work. The Avrami-Johnson-Mehl approach, further developed by Mittemeijer and co workers was employed to determine the activation energies for dissolution of GPI zones and β'' formation. The activation energy of dissolution of GPI zones is observed to increase with increasing level of cold work while that for formation of β'' decreases with increasing level of cold work. As expected, TEM showed strong interaction of strengthening precipitates with dislocations. The density of dislocation tangles is shown to increase with increasing degree of cold work.

1. Introduction

In the automobile industry, the use of aluminum alloys has increased over the years as manufacturers strive to design lighter vehicles as part of an overall goal to meet the North American Corporate Average Fuel Efficiency (C.A.F.E) Standards. These standards seek to improve fuel efficiencies and reduce vehicle emissions. Heat treatable AA6111 has emerged as one of the most prominent materials employed in outer body panels of cars and light trucks due to its unique combination of formability and paint bake strengthening characteristics.

There has always been the desire to have some way of estimating the yield strength of a part following forming and/or heat treatment operations. This is crucial since the dent resistance of a part is proportional to its yield strength and therefore high yield strength may be seen as beneficial. However, during stamping, high yield strength alloys tend to suffer spring back effect and inferior formability. For a formed and painted automobile panel, the yield strength involves combining strength components arising from cold work, strain aging, precipitation, and recovery. The conflicting demands of low yield strength alloy and high yield strength components in the 6xxx series alloys containing Cu are partially addressed through the aging response promoted through the automotive paint bake cycle. Unfortunately, only a small fraction of the full aging potential inherent in the alloy is exploited due to the relatively low temperatures and short duration of most commercial paint bake cycles. Typically, the paint bake curing cycle in the automobile manufacturing process involves: 10–20 min electro-coat (E-coat) curing at 170–185°C, 15–20 min primer curing at 160–170°C, and 15–25 min top/clear coat process at 130–150°C [1, 2]. The need for rapid strengthening response in today's finishing lines has led researchers to impose preaging treatments as well as other thermo-mechanical histories on 6xxx series aluminum alloys with the view to improving the strengthening characteristics as well as kinetics of these alloys [3–14].

*On Study Leave from, Physics Department, University of Cape Coast, Cape Coast, Ghana.
‡Author to whom all correspondence should be addressed.

In the present investigation, the effect of cold work on the precipitation kinetics of AA6111 is evaluated with a view to establishing its contribution to enhancing the paint bake response of the alloy as well as its aging kinetics, using methods that are compatible with industrial thermal practices for optimum results. The evaluation methods employed in the present study are tensile testing, differential scanning calorimetry (DSC), and transmission electron microscopy (TEM).

2. Experimental procedure

The composition limits of the material used in the present study, as received from Alcan International Limited, Kingston, Ontario, is presented in Table I. The material, supplied in the rolled state, was manufactured by a special technique, the details of which are reported in [15].

TABLE I Chemical composition limit of AA6111 (weight percent)

	Cu	Fe	Mg	Mn	Si	Ti	Al
Maximum	0.9	0.40	1.0	0.45	1.1	0.10	Balance
Minimum	0.5	0	0.5	0.10	0.6	0	

2.1. Tensile testing

The tensile test specimens were machined from a 1 mm thick stock sheet according to the ASTM E-8 standard, with a gauge length of 50 and 12 mm gauge width. These were then solution heat treated at $560 \pm 5^{\circ}$C for 30 min in an air furnace and quenched in 20°C water. Some of the as-quenched samples were given 2 or 5% cold work by stretching. All the specimens were then artificially aged at 180°C for various lengths of time. Subsequently, tensile tests were performed at room temperature using an Instron^{TM} screw- driven machine at a constant cross-head speed resulting in an initial strain rate of 0.025 min^{-1}. The yield strength, determined as the 0.2% strain offset, as well as the tensile strength were obtained from the resulting stress-strain plots.

2.2. Differential scanning calorimetry (DSC)

DSC analyses of samples subjected to various levels of cold work (0, 2, and 5%) by stretching were carried out using a temperature-modulated DSC 2910 system (MDSC^{TM}, TA Instrument Inc., USA), incorporating a refrigerated cooling system. The instrument was calibrated for enthalpy and temperature using a high purity elemental indium standard. Three DSC runs were conducted for each level of cold work in order to ensure reproducibility. All DSC runs began at 30°C and ended at 380°C at constant heating rates of 5, 10, 15 and 20°C min^{-1}. In order to correct for the additional heat flow arising from the difference in weight of the sample pan and the reference pan, and also to compensate for any asymmetry in the measuring system, a preliminary experiment was performed with commercially pure aluminum as blank. Thus the heat flow obtained was the difference between the measured and the blank values.

Peak temperatures for the various phases obtained in the DSC profiles for the above were extracted and used for preparation of TEM samples as follows: One set of thin foiled samples of AA6111 was run from 30°C to the GPI zone dissolution peak, at a heating rate of 10°C min^{-1}, held at this temperature for 15 min and quenched in cold water while another set was run from 30°C to the first largest exothermic peak temperatures at a heating rate of 10°C min^{-1}, held at the peak temperatures for 15 min and quenched in 20°C water to retain the phases formed at those temperatures. These were then stored for TEM studies.

2.3. Transmission electron microscopy (TEM)

TEM samples of AA6111 aluminum at the simulated paint bake cycle of 180°C for 30 min, peak aged for 10 h at 180°C, and simulated DSC runs conducted at 10°C min^{-1} to the GPI zone dissolution and the first largest exothermic peaks were examined in a Hitachi 2200 FE STEM at 200 kV. Thin foils were prepared by mechanical grinding, followed by an electro-polishing technique in a 30% HNO_3–70% methanol bath at a temperature between −30 to −20°C.

3. Results and discussion

3.1. Tensile results

Figs 1 and 2 show the variation of yield and tensile strengths as a function of aging time at 180°C for various levels of cold work. It can be seen in both graphs that as the aging time increases at each level of cold work, the yield and tensile strengths increase up to the peak value after which they decrease with further aging time. Thus, there is a significant increase in strength with increasing level of cold work. This can be attributed to the increase in dislocation density, due to cold work, piling up to form tangles and hence increasing the strength of the material. The time to reach peak yield strength

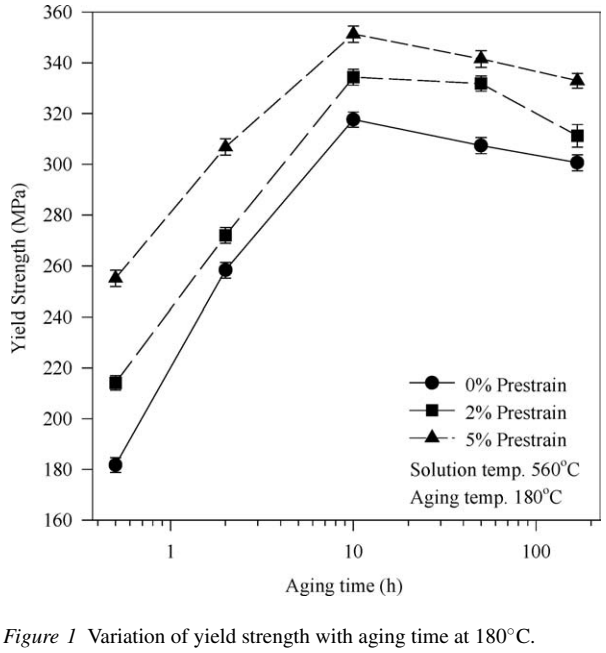

Figure 1 Variation of yield strength with aging time at 180°C.

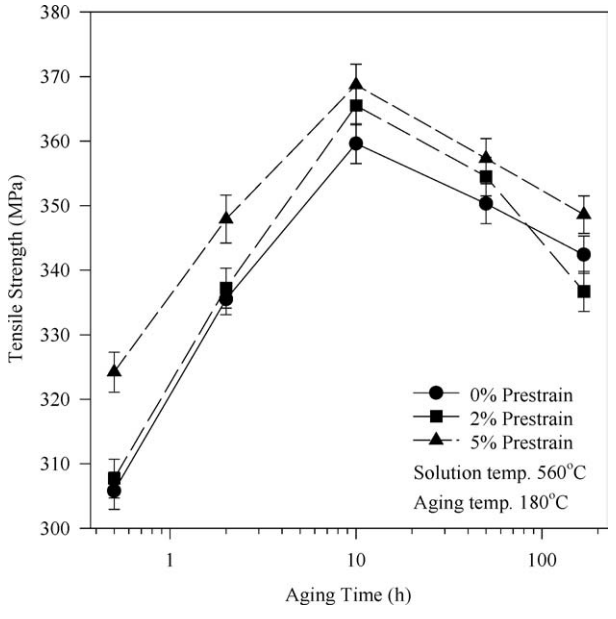

Figure 2 Variation of tensile strength with aging time at 180°C.

for all levels of cold work occurred after about 10 h of aging, indicating that the degree of cold work did not affect the time for the material to attain peak strength at 180°C. Under the simulated paint bake cycle (180°C for 30 min), it can be observed that there is a marked increase in the yield strength with increasing levels of cold work over that of unstrained sample, showing that cold working increases the overall dent resistance of the part. Fig. 3a and b show the bright field TEM micrographs of AA6111 samples at 0 and 5% cold work respectively, and artificially aged at 180°C for 10 h (peak time). The micrographs show that the unstrained sample comprises precipitates distributed randomly in the matrix. Fig. 3b on the other hand shows precipitates formed in a regular pattern, believed to be previous lines of dislocation generated by cold working. This illustrates that the increase in strength of the cold worked sample is due to increased amount of dislocations, which serve as high energy sites for the nucleation of precipitate particles.

3.2. Differential scanning calorimetry (DSC)

Differential scanning calorimetry (DSC) traces of the quenched and cold worked samples were obtained at scan rates of 5, 10, 15 and 20°C min^{-1} over the range of 30 to 380°C. Fig. 4 shows the DSC thermograms for the quenched and unstrained samples as well as those subjected to 2 and 5% cold work after quenching and a scan rate of 10°C min^{-1}. Fig. 5a and b show DSC traces at the above scan rates for the unstrained sample, and 5% cold worked sample respectively. In Figs 4 and 5, the reaction peaks correspond to the following phases: A corresponds to the GPI zone formation, B corresponds to GPI zone dissolution and C (the first large exothermic peak) corresponds to β'' formation. In each of the above plots the features of the thermograms remain generally the same, the peak reaction temperatures of the phases formed however vary with increasing level of cold work. This indicates that the reaction rates of formation of the various phases differ with imposed level of cold work as well as scan rate.

Fig. 6 shows the variation of peak reaction temperature for GPI zone dissolution and formation of the β'' phase with level of cold work at the scan rate of 10°C min^{-1}. It can be observed that the peak reaction temperatures for GPI zone dissolution as well as formation for the β'' peak shift to lower temperatures, indicating the ease of formation, and thus a faster rate of formation of these phases with increasing level of cold work. This, unlike that reported by Papazian [16] in which a shift to higher temperatures was observed for other aluminum alloys and attributed to an increase in average cluster size, demonstrates the fast response of the kinetic reaction with increased level of cold working in the AA6111 alloy.

The precipitation sequence for Cu-containing Al-Mg-Si alloys following super saturated solid solution (SSS) has for a long time been considered to be analogous to the ternary Cu-free Al-Mg-Si alloys shown in Equation 1:

$$\text{SSS} \rightarrow \text{GPI} \rightarrow \beta'' \rightarrow \beta' \rightarrow \beta\,(\text{Mg}_2\text{Si}) \qquad (1)$$

However, Gupta and co-workers [17] in their earlier study of the precipitation sequence in AA6111 (an Al-Mg-Si-Cu alloy) proposed another possible sequence that could be followed as:

$$\text{SSS} \rightarrow \text{GPI} \rightarrow \theta'' \rightarrow \theta' \rightarrow \theta\,(\text{Al}_2\text{Cu}) \qquad (2)$$

Recently, the precipitation of the quaternary Q phase and its precursor Q′ in Cu-containing Al-Mg-Si has become increasingly clear [18–23]. As a result, the precipitation sequence in AA6111 has come to be accepted as:

$$\begin{aligned}\text{SSS} &\rightarrow \text{clusters/GP zones} \rightarrow \beta'' + \text{Q}' \\ &\rightarrow \text{equilibrium Q} + \beta(\text{Mg}_2\text{Si}) \end{aligned} \qquad (3)$$

The extent of reaction at a given temperature during a DSC scan can be controlled by thermodynamic equilibrium or by kinetic limitations [24]. Fig. 7a and b shows the effect of DSC heating rate on the peak reaction temperature for dissolution of GPI zones and formation of the first large exothermic peak respectively, for various levels of cold work (0, 2, and 5%). It is apparent from the results in Fig. 7a and b that increasing the DSC heating rate causes the peaks to occur at systematically higher temperatures. This indicates that precipitate formation in the alloy under this varying heat rate condition is a function of temperature and time.

The activation energy for GPI dissolution and formation of the first large exothermic peaks can be estimated by applying the relationship developed by Mittemeijer and co-workers [25, 26], which is given as

$$\ln\left(T_\text{p}^2/\phi\right) - Q/(RT_\text{p}) = A \qquad (4)$$

where A is a constant, ϕ denotes the DSC heating rate (K min^{-1}), Q, the activation energy, R, the gas constant

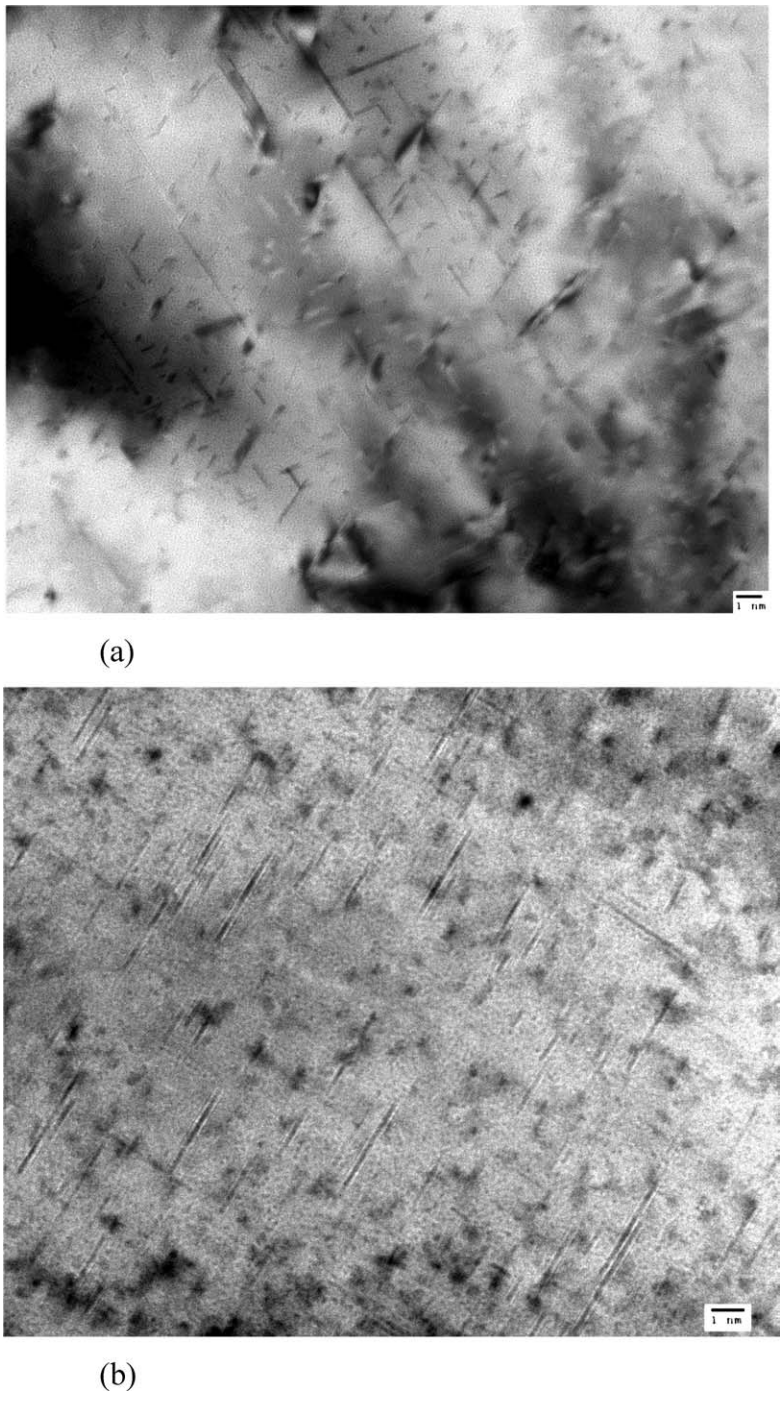

Figure 3 Bright field TEM micrograph of (a) unstrained sample and (b) 2% cold worked alloy subjected to 180°C artificial aging for 10 h.

(=8.314 J mol^{-1} K^{-1}), and T_p, the temperature where the maximum transformation rate is experienced during DSC scan (K). An assumption is made at this point that the peaks produced at the different scan rates in the DSC represent the same transformation product. In a constant heating rate DSC experiment, T_p is usually taken to be approximately equal to the peak reaction temperature. Hence, the activation energy can be calculated from the slope of the straight line obtained by plotting $\ln(T_p^2/\phi)$ versus $1/T_p$.

Figs 8 and 9 show plots after Equation 4 for various levels of cold work for the GPI zone dissolution and β'' formation respectively. Table II presents a summary of the level of cold work, peak reaction temperature and the corresponding activation energies for the resultant GPI zone dissolution and β'' formation respectively. Examining Table II shows a general trend of increase in the activation energy for GPI zone dissolution with increasing level of cold work in the alloy. This can be explained as follows. Prior cold work tends to stimulate and speed up the conversion of solute clusters to GPI zones during the early stages of subsequent DSC scan. This results in reduction in the clusters formed and their sizes as well as an increase in the vacancy concentration within the individual clusters, setting up a high binding energy between the GPI zones and vacancies as proposed by Lutts [27] and also by Hupper and Hornbogen [28]. Thus, a lot more energy is required

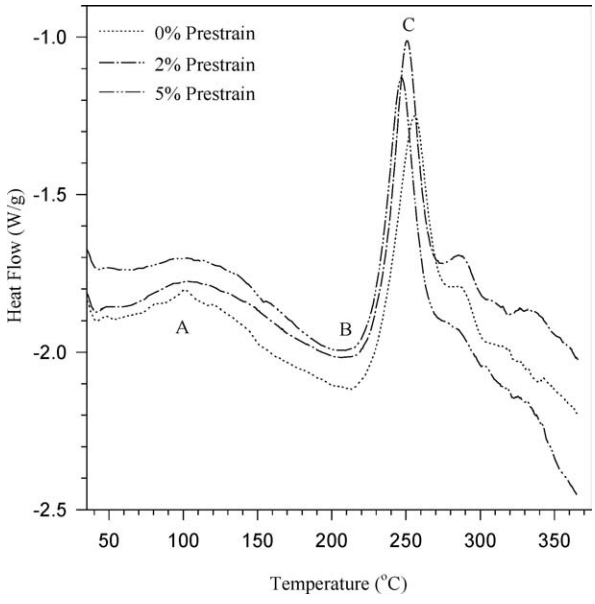

Figure 4 DSC thermograms of quenched samples of AA6111 at various levels of cold work.

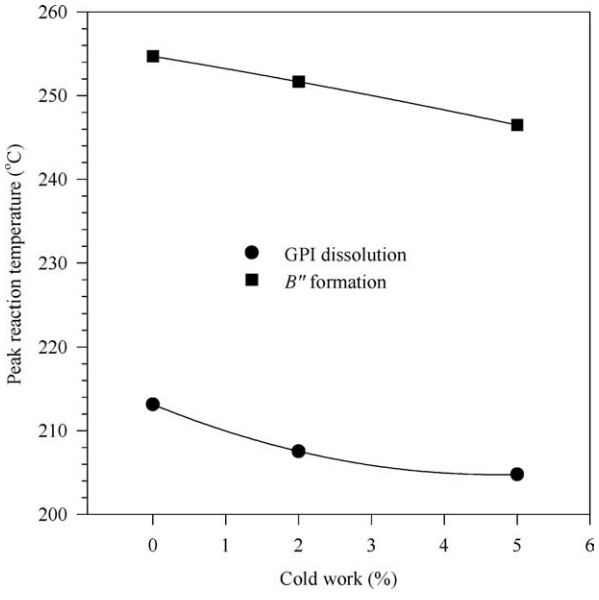

Figure 6 Variation of peak reaction temperature with cold work for GPI dissolution and β'' formation.

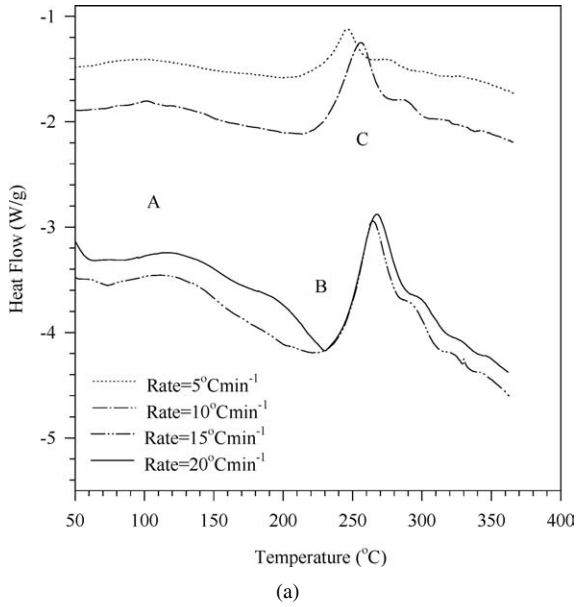

(a)

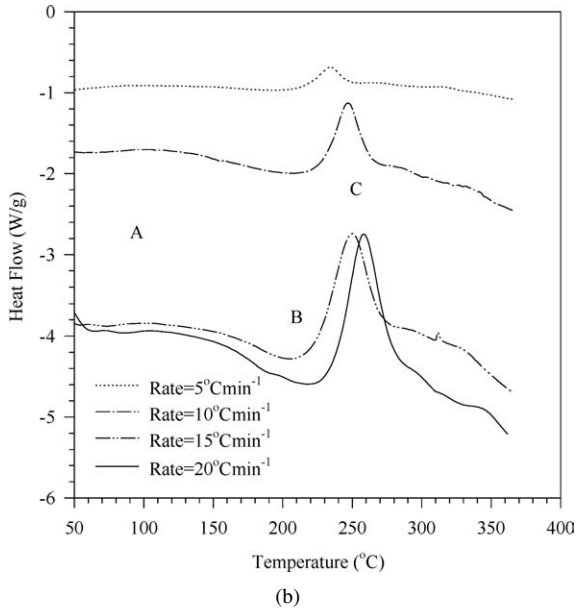

(b)

Figure 5 DSC thermograms of (a) 0% and (b) 5% cold worked samples at various scan rates.

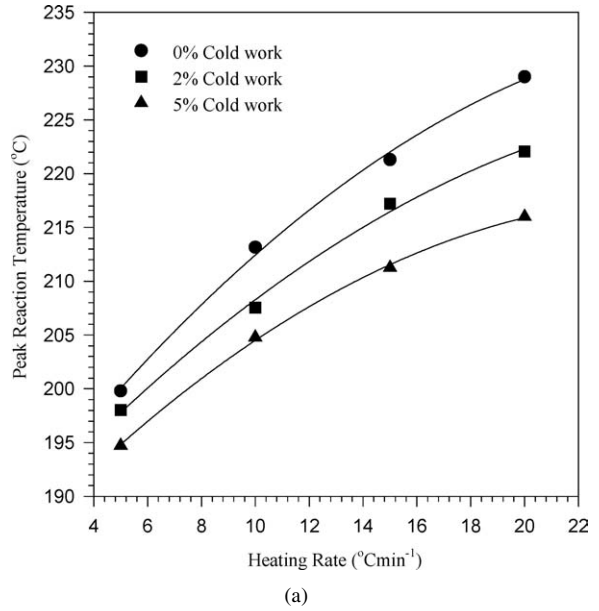

(a)

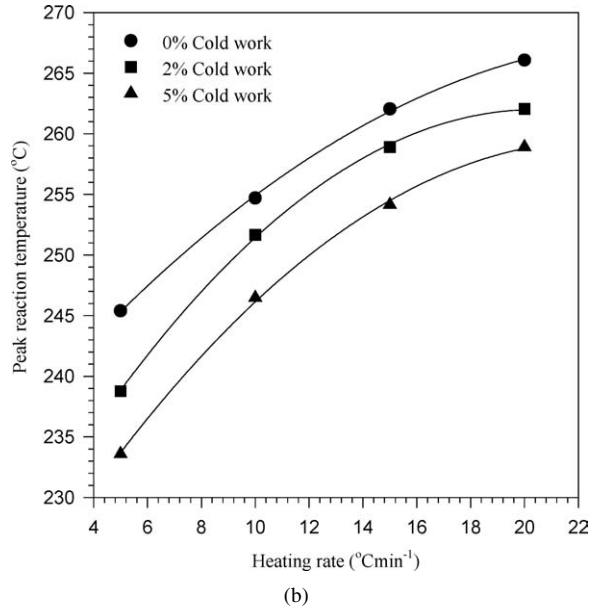

(b)

Figure 7 Variation of peak reaction temperature with heating rate at various levels of cold work for (a) GPI dissolution and (b) β'' formation.

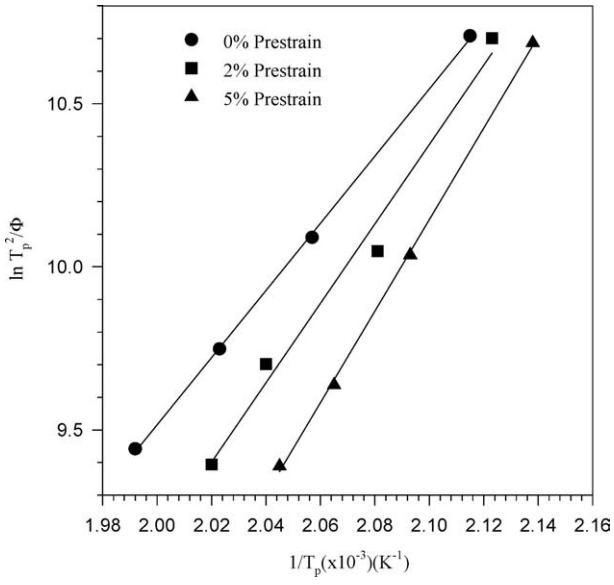

Figure 8 Plot after Equation 4 for determination of activation energy for GPI dissolution.

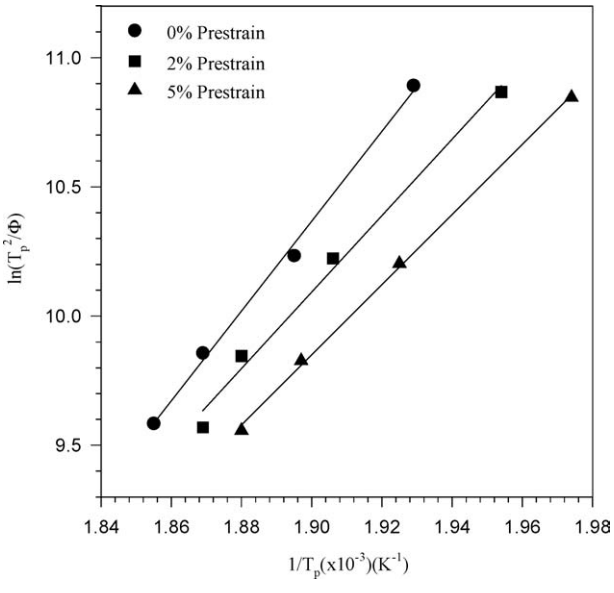

Figure 9 Plot after Equation 4 for determination of activation energy for β'' formation.

for dissolution of the GPI zones with increasing levels of cold work consistent with the trend shown. The dissolution of clusters and GPI zones during DSC scan has a direct impact on the subsequent precipitation of β'' in AA6111 aluminum alloys. From Table II, the activation energy of formation of β'' shows a decreasing trend with increasing level of cold work. At 0% cold work the activation energy of formation of β'' was estimated to be $\sim$146 KJ mol^{-1}. This is consistent with values reported by Shercliff and Ashby [29] in AA6061 alloy. Upon application of 2% cold work the activation energy decreased to $\sim$120 KJ mol^{-1} and further decreased to $\sim$114 KJ mol^{-1} upon application of 5% cold work. The decreasing trend is indicative of the fact that less energy is required for the formation of β'' with increasing level of cold work and hence a faster response to the precipitation kinetics in the alloy, corroborating the earlier results of DSC in Figs 5 and 6.

TABLE II Activation energy for GPI dissolution and β'' formation determined after Equation 4

	GPI dissolution		β'' formation	
Cold work (%)	Peak temperature (10°C min^{-1})	Activation energy (kJ mol^{-1})	Peak temperature (10°C min^{-1})	Activation energy (kJ mol^{-1})
0	213.2	85.6	254.7	146.9
2	207.5	104	251.7	119.9
5	204.8	116	246.5	114

To better understand the results of activation energy obtained from DSC and the transformation events associated with them under cold work conditions, specimens of the samples cold worked to the various levels were heated at a standard scan rate of 10°C min^{-1} in a DSC up to the β'' peak, whereupon they were held at that temperature for 15 min and rapidly quenched in cold water. The temperatures chosen for the occurrence of the β'' precipitates were 256, 251 and 246°C for the corresponding levels of cold work of 0, 2, and 5% respectively. TEM was then performed on the samples under this condition.

Fig. 10a and b show the bright field TEM micrographs of the unstrained and the 5% cold worked samples following the simulated DSC scan up to temperatures of 256 and 251°C respectively. In Fig. 10, a regular distribution of lathe like strengthening precipitates is observed for the unstrained sample while the 5% cold worked sample shows random distribution of strengthening precipitates along dislocations in tangles. The amount of strengthening precipitates is also higher in the cold worked samples compared to that observed in the unstrained sample, supporting the observations made in the tensile as well as DSC results. Thus cold working has been shown to improve the kinetics for precipitation as well as the mechanical properties of the alloy.

4. Conclusions

The application of increasing levels of cold work to AA6111 has been shown to significantly improve the yield strength of the alloy and hence its dent resistance characteristics.

DSC results show a faster response of the kinetic reactions in AA6111 with increasing level of cold work, and an improvement in the mechanical strengthening characteristics of the alloy under the current paint bake cycle employed in industry. The activation energy for dissolution of GPI zones has been observed to increase with increasing levels of cold work. This is attributed to a reduction in the clusters formed, their sizes as well as an increase in the vacancy concentration within the individual clusters, which set up a high binding energy between the GPI zones and vacancies. The activation energy of formation of the β'' phase on the other hand decreases with increasing level of cold work and this is attributed to the high energy states induced in the material as a result of cold working, leading to less energy required for the formation of the β'' phase.

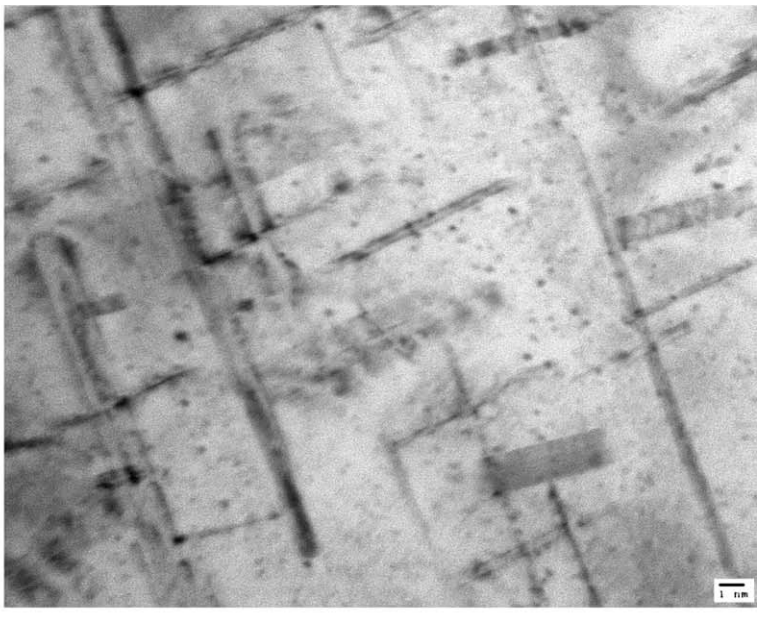

(a)

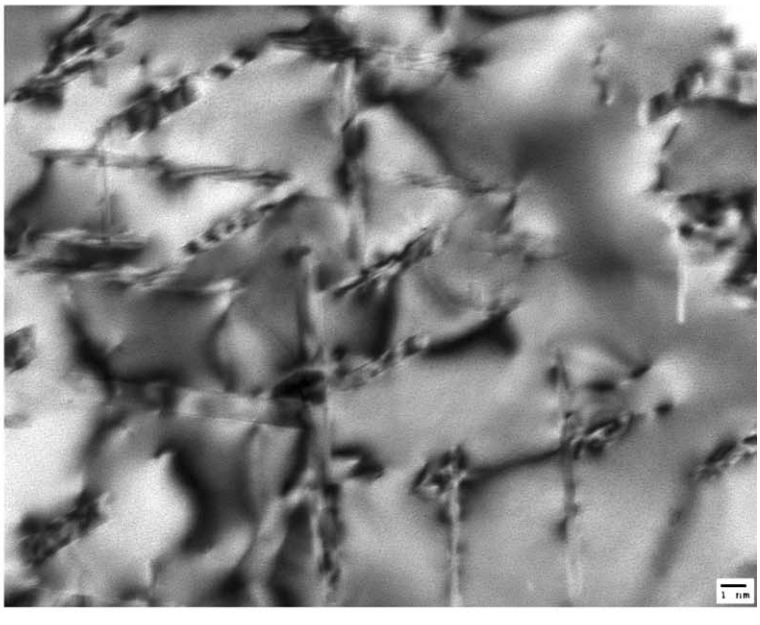

(b)

Figure 10 Bright field TEM micrograph of AA6111 following the application of a simulated DSC scan up to (a) 256°C and (b) 251°C.

Acknowledgement

The authors would like to thank Dr. A. K. Gupta of Alcan International Limited, Kingston, Ontario for his technical contribution. Government of Ghana Scholarship through the University of Cape Coast and the University of Saskatchewan Graduate Student Scholarship to G. K. Quainoo are gratefully acknowledged. Financial assistance from the Natural Sciences and Engineering Research Council of Canada (NSERC) in the form of a research grant to S. Yannacopoulos is hereby acknowledged.

References

1. A. K. GUPTA, D. J. LLOYD and M. J. BULL, SAE International Congress & Exposition (1996), SAE Paper No. 960164.
2. M. MURAYAMA and K. HONO, *Acta Mater.* **47** (1999) 1537.
3. S. B. KANG, L. ZHEN, H. W. KIM and S. T. LEE, in Proc. 5th Int. Conf. on Al Alloys, Grenoble, France, 1996 (Transtec Publication Ltd., Zuerich, Switzerland, 1996) p. 827.
4. M. SAGA, Y. SASAKI, M. KIKUCHI, Z. YAN and M. MATSUO, in Proc. 5th Int. Conf. on Al Alloys, Grenoble, France, 1996 (Transtec Publication Ltd., Zuerich, Switzerland, 1996) p. 821.
5. P. BARCZY and F. TRANTA, *Scand. J. Met.* **4** (1975) 284.
6. T. HIRATA and S. MATSUO, *Trans. J. Jpn. Inst. Met.* **13** (1972) p. 231.
7. R. C. DORWARD, *Metall. Trans.* **40** (1973) 507.
8. H. SUZUKI, M. KANNO and G. ITOH, *J. Jpn. Inst. Met.* **30**(11) (1980) 609.
9. M. YAMAGAWA, M. ABE and S. OHIE, *ibid.* **46**(1) (1996) 27.
10. M. TAKEDA, F. OHKUBO, T. SHIRAI and K. FUKUI, in Proc. 5th Int. Conf. on Al Alloys, Grenoble, France, 1996 (Transtec Publication Ltd., Zuerich, Switzerland, 1996) p. 815.
11. J. D. BRYANT, *Metall. Mater. Trans.* A **30A** (1999) 1999.
12. W. F. MIAO and D. E. LAUGHLIN, *ibid.* **31A** (2000) 361.

13. J. D. BRYANT, H. KUNG and A. MISRA, in "Automotive Alloys II," edited by S. K. Das (The Minerals, Metals & Materials Society, 1998) p. 3.
14. J. D. BRYANT, Automotive Alloys, in Proc. of TMS Annual Meeting of 1997, edited by S. K. Das (1999) p. 19.
15. G. BURGER, A. K. GUPTA, P.W. JEFFREY and D. J. LLOYD, *Mater. Char.* **33** (1995) 23.
16. J. M. PAPAZIAN, *Metall. Trans.* A **12A** (1981) 269.
17. A. K. GUPTA, P. H. MOROIS and D. J. LLOYD, in Proc. 5th Int. Conf. on Aluminum Alloys, Grenoble, France, 1996 (Transtech, Zuerich-Uetikon, Switzerland, 1996) p. 801.
18. W. F. MIAO and D. E. LAUGHLIN, *Metall. Mater. Trans.* A **31A** (2000) 361.
19. *Idem.*, *Scripta Mater.* **40**(7) (1999) 873.
20. K. M. ENTWISTLE, J. H. FELL and K. I. KOO, *J. Inst. Metals* **91** (1962–63) 84.
21. A. K. GUPTA and D. J. LLOYD, "Aluminum Alloys: Their Physical and Mechanical Properties, edited by L. Arnberg *et al.* (Norwegian Institute of Technology and SINTEF Metallurgy, Trondheim, 1992) Vol. 2, p. 21.
22. D. J. LLOYD, D. R. EVANS and A. K. GUPTA, *Canadian Metall. Quart.* **39**(4) (2000) 475.
23. M. W. MAHONEY and P. J. DYNES, *Scr. Metall.* **19** (1985) 539.
24. E. J. MITTEMEIJER, LIU. CHENG, P. J. VAN DER SCHAAF, C. M. BRAKMAN and B. M. KOREVAAR, *Metall. Trans.* A **19A** (1988) 925.
25. E. J. MITTEMEIJER, A. VAN GENT and P. J. VAN DER SCHAAF, *ibid.* **17A** (1986) 1441.
26. A. LUTTS, *Acta Metall.* **19** (1961) 577.
27. G. HUPPER and E. HORNBOGEN, in Proc. 4th Int. Conf. on Al Alloys, Atlanta, GA, 1994 (Georgia Instutute if Technology, Atlanta, Georgia, 1994) Vol. 1, p. 628.
28. H. R. SHERCLIFF and M. F. ASHBY, *Acta Metal* **38**(10) (1990) 1789.

Received 18 August 2003
and accepted 3 June 2004